Critical flux-based membrane fouling control of forward osmosis: Behavior, sustainability, and reversibility

Thanh-Tin Nguyen, Seungho Kook, Chulmin Lee, Robert W. Field[*], In S. Kim[**]

Global Desalination Research Center (GDRC), School of Earth Sciences and Environmental Engineering, Gwangju Institute of Science and Technology, 123 Cheomdangwagi-ro, Buk-gu, Gwangju 61005, Korea

[*]Department of Engineering Science, University of Oxford, United Kingdom

[**] Corresponding author.

In S. Kim

Email: iskim@gist.ac.kr

Telephone: +82-62-715-2477

Fax: +82-62-715-2434

Abstract

Membrane fouling is closely related to the concept of critical flux. Therefore, a fouling control stategy for forward osmosis (FO) membranes that is based on the critical flux is necessary. This study systematically investigated the critical flux behavior of FO membranes (CTA and PA-TFC) in the short-term using a stepping method (draw solution (DS) concentration stepping). In addition, to test the reliability of this method, long-term experiments were conducted to evaluate the influences of operational critical flux on the fouling behavior (sustainable operation and fouling reversibility/irreversibility), thereby determining the critical flux for reversibility. Our results showed that the DS concentration stepping could be applied for critical flux determination in FO. Both membranes exhibited higher critical flux values for alginate fouling compared to other single foulants such as colloidal silica or gypsum. The values were 15.9 LMH for a cellulose triacetate membrane (CTA) and 20.5 LMH for the polyamide thin-film composite (PA-TFC). Whilst these values should be adequate in FO applications they were determined for single foulants. The presence of multispecies of foulants caused a significant decline in the critical flux values. This study found 5.4 LMH for the CTA membrane and 8.3 LMH for the PA-TFC membrane for the combined foulants of alginate + gypsum. This indicates that the critical flux behavior in FO was dependent on the foulant type and membrane type. Importantly, 98-100% restoration of water flux was achieved with the PA-TFC membrane at an operation either close to or below critical flux (i.e., in case of negligible fouling), except for the combination of alginate-combined colloidal silica. The critical fluxes for reversibility obtained in this study will aid the efficient operation of practical FO processes.

Keywords: Critical flux; Single foulant; Combined foulant; Forward osmosis membrane; Critical flux for reversibility.

1. Introduction

Forward Osmosis (FO) is an osmotically driven membrane process in which water is transported from low osmotic pressure (feed solution) to high osmotic pressure (draw solution) across the semipermeable membrane through the action of a chemical potential gradient [1]. Hybrid FO processes have recently emerged as possible systems for the simultaneous treatment of impaired/reclaimed water and seawater for reuse [2] [3] [4] [5] since standalone FO process cannot economically achieve either water treatment or desalination of seawater. These hybrid processes can bring many advantages regarding the energy consumption and the water quality: i) decrease of desalinated energy cost because seawater is diluted before entering RO desalination, ii) reduction of the fouling propensity of the RO stage through pretreatment of impaired water; (iii) a multi-barrier protection is established to improve contaminant removal; thereby giving opportunity for safe and high-quality reuse of impaired water [5] [6] [7]. In detail, complex wastewater (i.e., raw sewage, primary effluent, secondary effluent, biologically treated wastewater effluent) can be directly pre-treated by FO process (i.e., pre-treated wastewater or pre-concentrated wastewater) and subsequently potable water can be produced by combining with a draw solute recovery process (i.e., reverse osmosis or membrane distillation) [8] [9]. Despite less impact of fouling compared to RO (i.e. due to the absence of hydraulic pressure) the performance and large-scale implementation of FO process can be significantly affected by fouling [10]. The fouling, or to be more precise, the flux decline occurring with an FO membrane is generally considered to be less severe than that with a RO membrane. This has been attributed by some to the absence of applied hydraulic pressure; the foulant layer on a FO membrane is said to be looser whereas that on an RO membrane is said to be more densely compacted [11]. On the other hand others have found no difference in flux decline between FO and RO fouling, and attributed this to the low starting flux which was said to be below the critical flux [12]. Others have specifically suggested that foulant layer compaction

is physically related to water flux not hydraulic pressure [13] ADD [new ref]. Three major types of fouling occur in the FO membrane: (1) organic fouling caused by macromolecular organic compounds as polysaccharides, protein, and humic acid; (2) inorganic fouling involving the scaling with the crystallization of sparingly soluble mineral salts and colloidal fouling with the deposition of particles; (3) biofouling from bacteria attachment [14].

Membrane fouling is closely related to the concept of the critical flux, which was originally introduced by several authors [15] [16] [17], who reported: “below the critical flux, fouling occurs insignificant, whereas, above the critical flux, fouling becomes more severed”. Therefore, the critical flux concept has been widely introduced to the full range of pressure-driven membrane processes, including microfiltration (MF) [18], ultrafiltration (UF) [19] [20], nanofiltration (NF) [21] [22] and even in RO [23] [24], to control fouling in desalination and water treatment processes. An operation below a critical value, called critical flux (where the distinction is between no fouling and fouling) or threshold flux (where the distinction is between low fouling and more extensive fouling) is favorable to the control of membrane fouling and thus the maintenance ofsustainable operation [25]. Membrane fouling comprises reversible and irreversible fouling, the difference being based on the degree of attachment of foulants to the membrane surface. This is a vital assessment to quantify the fouling propensity as well as the potential recovery of water flux. A sufficient shear force (i.e., physical flushing) can be used for the removal of reversible fouling but this is not the case with irreversible fouling. Numerous authors have investigated the fouling reversibility of FO under various scenarios: single fouling (i.e., alginate [26] [27], colloidal silica [26] [27], gypsum scaling [14] [28] [29], combined fouling (i.e., alginate + colloidal silica [27], alginate + gypsum scaling [14]), different membrane types [28] [30], and operating condition (i.e., effect of applied hydraulic pressure [27] [31]). Their results indicated that a higher restoration of

water flux is obtained with single foulants. Nevertheless, the effect of various initial fluxes (achieved by varying DS concentration) on the fouling reversibility has not been fully explored yet. The critical flux for reversibility has previously been introduced for pressure-driven process; efficiency and economical operation are favoured by operation below this value [32]. Thus, this concept is also expected to be applicable in FO membrane processes. To determine the critical flux, several methods can be used: flux–pressure profile, flux stepping, flux cycling, mass balance, and fouling rate analysis [32]. In particular, the stepping method is commonly used in pressure-driven membrane processes for critical flux determination, in which either the transmembrane pressure (TMP) or the flux is increased stepwise, and the response (either flux or TMP) is observed [32] [33].

Nevertheless, hitherto, little attention has been directed to the role of the critical flux of osmotically driven processes (FO) in controlling membrane fouling compared to that of pressure-driven processes (RO, NF, and UF). For instance, several authors have investigated the critical flux governing the fouling in the FO membrane through observations and experiments (Table 1) [34] [35] [36]. These studies have not systematically investigated the various fouling scenarios essential for applications such as the simultaneous treatment of impaired water for reuse and seawater desalination. In addition, past studies have focused on studying the commercial membranes principally those with low tomoderate permeability from HTI (i.e. their, cellulose triacetate (CTA) and thin film composite (TFC)). However, a newly developed polyamide thin-film composite (PA-TFC) from the Toray company was recently introduced as a potential candidate for the practical application due to its high permeability [37] [38] [39]. Therefore, a comparison of critical flux behavior between the former and latter membrane is essential to aid membrane selection. Moreover, as aforementioned, critical flux for reversibility is definitely beneficial but previous

studies (Table 1) have not performed the essential long-term evaluation. Therefore our work included a systematic study on the critical flux behavior in longer term operation whilst also comparing: CTA from HTI Company with PA-TFC membrane from Toray Company.

As mentioned above the stepping method is well known for the characterization of critical flux in pressure-driven processes. This was adapted for the current study. Instead of using pressure stepping (or flux stepping), the draw solution (DS) concentration stepping method (0.25–3 M) was used for the critical flux determination in various FO fouling scenarios under the short-term test. Moreover, to test the reliability of the DS concentration stepping method in this study, an essential investigation of the sustainability of the water fluxes was also performed in a series of long-term tests. These were run to determine membrane fouling behavior above the determined value of critical flux, at critical flux, and below critical flux. Additionally, in the current study, to solve the gap of the previous studies as mentioned beforehand, an assessment of the fouling reversibility around critical flux conditions was also made in order to determine the critical flux for reversibility.

Table 1. Summary of previous studies related to critical flux in FO membranes

Test method	Application	Foulant	Membrane	Results	Reference
Fouling surface coverage using direct microscopic observation through the me	Membrane-based seawater desalination	Latex microparticles (3 µm)	Cellulose Triacetate (CTA) flat sheet membrane (HTI)	FO critical flux for latex filtration was approximately 28 LMH. AL-FS orientation more fouling resistant than AL-DS. Feed spacer was able to considerably enhance initial flux and critical flux in FO (> 52 LMH)	[34]
Stepping method: Flux stepping (concentration stepping)	Membrane-based microalgae filtration	Microalgae 100 mg/L	Cellulose Triacetate (CTA) flat sheet membrane (HTI)	FO critical flux was between 9.3 and 15.5 LMH. Stable flux can be obtained by operating below the critical flux. Fouling was more severe and less reversible due to the presence of divalent ions (Mg^{2+}). A higher critical flux of 21 LMH was obtained with spacers in the feed channel	[35]
Long-term test: Flux decline observation	Membrane-based seawater desalination	Humic acid: 200 mg/L Alginate: 200 mg/L	Cellulose triacetate (CTA), thin-film composite (TFC) FO membrane (HTI) and TFC FO (Porifera Inc.)	Low-fouling behavior observed in FO (AL-FS), while operating at lower permeation of 10 LMH.	[36]

2. Materials and methods

2.1. FO membranes and characterization

FO membranes used in the current study include the CTA membrane from Hydration Technologies Inc., USA and a PA-TFC membrane from Toray Chemical Korea Inc., Korea. The CTA membrane was fabricated from cellulose acetate embedded in a polyester woven mesh [14]. Meanwhile, the PA-TFC membrane consisted of a selective polyamide active layer formed by interfacial polymerization on top of a polysulfone porous substrate [39]. Prior to experimental use, the FO membranes were soaked in deionized (DI) water and stored at 4 °C. For the membrane characterization, a cross-section of the pristine membrane was used to determine its thickness and the membrane morphology was analyzed using a high-resolution field-emission gun scanning electron microscope (FE-SEM), LEO Ge- mini 1525 (Carl Zeiss). The contact angle, determined using the sessile drop approach (Kruss G10 goniometer, Kruss, Germany), was used to characterize the hydrophobicity/hydrophilicity. The roughness of the membranes was determined using atomic force microscopy (AFM). To measure the A, B and S parameters, this study followed the procedures of the previous works [38] [40]. In detail, water permeability (A) and solute permeability (B) were determined using a pressure-driven filtration unit whilst structural parameter (S) was defined using an osmosis-driven filtration unit. For the permeability test, a stable water flux was obtained after membrane compaction test (10 bar) using DI within 2 hours. Afterwards, under an applied hydraulic pressure of 10 bar with 2000 ppm NaCl solution, water and solute permeability were determined by measuring the mass of permeate and NaCl rejection. For osmosis-driven filtration unit, water flux was measured in FO mode with DI (feed solution) and NaCl solution as draw solution (with concentrations of 0.1, 0.2, 0.5 and 1.0 M). The S parameter was calculated from the data, the pre-determined A and B values, following the equations given in a previous study [40].

166 The specific properties of the membranes including water permeability (A), solute permeability
167 (B), thickness, hydrophobicity/hydrophilicity, surface roughness, are detailedin Table 2. The
168 average roughness of PA-TFC and CTA are 50.5 mm and 23.9 nm, respectively, suggesting that
169 the PA-TFC membrane has a rougher active layer surface. The lower contact angle of the PA-TFC
170 indicates a more hydrophilic surface.

171 **Table 2.** Specific membrane properties

Properties		**CTA**	**PA-TFC**
Membrane thickness (μm)		59.3 ± 24.0	91.4 ± 1.3
Average surface roughness (nm)	Active layer	23.9 ± 8.9	50.5 ± 2.2
	Support layer	11.1 ± 1.6	20.4 ± 3.4
Hydrophobicity (°)	Active layer	50.0 ± 2.4	40.3 ± 2.4
	Support layer	58.1 ± 0.3	48.4 ± 0.7
Water permeability (A) (LMH Bar^{-1})		0.821	8.818
Solute permeability (B) (m s^{-1})		1.672×10^{-7}	2.457×10^{-7}
Structure parameter (S) (μm)		477 ± 30	276 ± 13

172

173 **2.2. Model foulants**

174 The model foulants used for the fouling experiments consist of sodium alginate, colloidal silica,
175 and gypsum scaling, which represent the primary constituents of the major inorganic and organic
176 components in wastewater effluent or surface water. Sodium alginate was used as the organic
177 foulant; it consists of polysaccharides, in the molecular weight range of 12–80 kDa and is
178 negatively charged [41]. It was obtained in powder form from Sigma–Aldrich, USA. Prior to
179 introducing it into the feed solution (FS), 2 g/L of the sodium alginate stock solution was prepared
180 by completely dissolving the powder in DI water for 24 h before keeping it at 4 °C. Colloidal silica
181 (Snowtex ST-ZL) supplied by Nissan Chemical Industries, Tokyo, Japan, was used to represent
182 the suspended colloidal matter. An average particle size of 139 nm was detailed by Bo et al. [42],
183 for a colloidal suspension containing 40% w/w amorphous silica and 60% w/w water. The colloidal
184 silica was stirred for 1 h to achieve complete dispersion before its use in the feed solution. With

185 regard to gypsum scaling experiments, stock solutions of 1 M $CaCl_2$ and 1 M Na_2SO_4, were
186 vigorously mixed for 24 h and then kept at 4 °C.
187
188 **2.3. Feed and draw solutions**
189 The FS used contained 10-mM NaCl for the baseline experiment and the fouling experiments. The
190 concentration of foulants in the feed solution was fixed at 200 mg/L and 1,000 mg/L for alginate
191 and silica, respectively whilst gypsum scaling was formed from 20-mM Na_2SO_4 and 20-mM $CaCl_2$.
192 The foulant concentrations were introduced either for single fouling or mixed fouling. To avoid the
193 effect a changes in the total ionic strength (IS) on flux behavior, the total IS was maintained at 0.13
194 M . To achieve this in the short-term operation (section 2.5) a fresh feed solution was prepared for
195 each step of DS concentration.. In brief, the detailed compositions of the FS for the baseline
196 experiment and fouling experiments are listed in Table 3. The FS pH was retained at 7.05 ± 0.03
197 using either 0.1-M NaOH solution or 0.5-M HCl solution. The concentration range of the NaCl DS
198 (0.25–3 M) was adjusted based on the experimental protocol of the short-term critical flux
199 determination experiment (described in detail in section 2.5).
200 **Table 3.** Components of feed solution for baseline and fouling experiments

Foulants	NaCl (mM)	Silica colloid (mg/L)	Alginate (mg/L)	Na_2SO_4 (mM)	$CaCl_2$ (mM)	IS Total (M)
Baseline experiment	10	0	0	40	0	0.13
Alginate	10	0	200	40	0	0.13
Colloidal silica	10	1000	0	40	0	0.13
Gypsum	10	0	0	20	20	0.13
Alginate + Colloidal silica	10	1000	200	40	0	0.13
Alginate + Gypsum	10	0	200	20	20	0.13

201 IS: Ionic Strength
202 **2.4. Lab-scale FO system setup**

Fig. 1 shows a schematic diagram of the lab-scale FO system. The system was operated in the cross-flow mode for all experiments. An acrylic FO cell consisting of two rectangular channels with dimensions of 75 mm (length) × 25 mm (width) × 3 mm (height) and an effective filtration area of 1875 mm^2, was used to evaluate water permeation. No spacer was used for both the feed and draw channels of the FO cell. A similar cross-flow velocity (CFV) of 6.66 cm/s using flow meters was maintained in both the feed and draw channels. Circulation in counter-current mode was maintained using a magnetic drive gear pump (GAF-T23-DEMSE MICROPUMP Inc., USA). For the physical cleaning experiment, a high CFV of 13.32 cm/s was imposed on the feed side for 30 min with DI water. Additionally, to check the maintenance of the FO mode, pressure gauges were installed in the DS and FS channels. The temperature was maintained at 23±1 ^oC for the FS and DS using a water bath. An electronic mass balance (GF-6100, A&D Company, Japan) was used to record the variation in the DS mass to enable the calculation of the water flux.

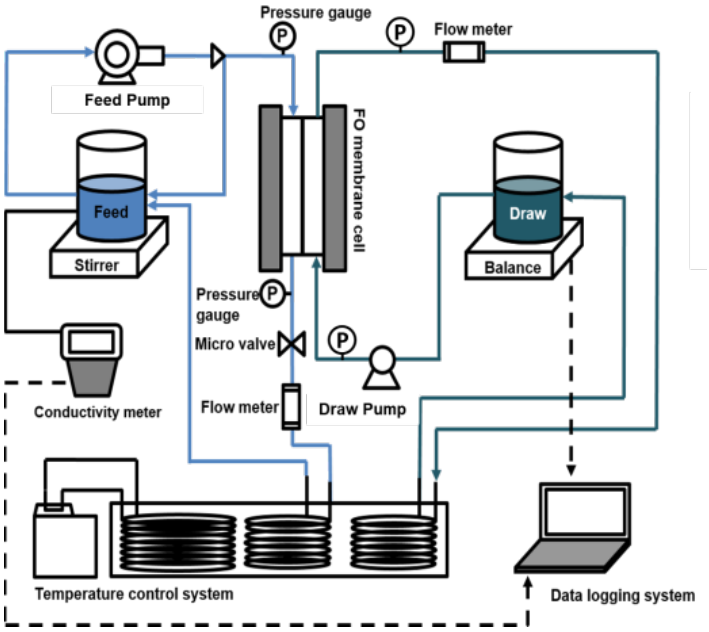

Figure 1. Schematic diagram of lab-scale FO system

2.5. Short-term critical flux determination experiment

For a typical critical-flux determination experiment, a membrane was placed in the test cell and CFV adjustments of the DS and FS were made to reach the desired value of 6.66 cm/s. The DS and FS were prepared with the same volume of 2 L. A stabilization testing for 30 min was performed using DI water for both the FS and DS sides prior to the stepping experiments. Then DS concentrations of 0.25-, 0.5-, 1.0-, 1.5-, 2.0-, and 3.0-M NaCl were employed consecutively to conduct the DS concentration stepping method. Each test included the baseline stage (without foulant) followed by the fouling stage. A difference between the two stages was the presence of foulants in the FS in the latter stage. To avoid the influence of excessive DS dilution and FS concentration, which may change the osmotic pressure, a stepping duration of 30 min was selected from the study of Zou et al. [43]. Consequently, in every minute only 0.17–0.68 mL (CTA membrane) and 0.29–1.26 mL (PA-TFC membrane) with respect to the DS concentration of 0.25–3 M was permeated into 2 L of the DS; therefore such weak dilutions have a negligible effect. A membrane orientation with the active layer facing the FS (AL-FS) was applied throughout all tests.

2.6. Long-term FO fouling experiment

To check the reliability of the DS concentration stepping method for the critical-flux determination in the FO membrane, a long-term experiment was conducted to evaluate the influences of operational critical flux on the fouling behavior including fouling reversibility/irreversibility. From the critical flux value determined from the short-term experiments, operations above value, at this value, and below this value were investigated for various fouling scenarios for both the CTA and PA-TFC membranes (Table S-1). Similar to the short-term test, a FO test using DI water on both the DS and FS sides was conducted to stabilize the system for the 30 min prior to the baseline experiments. As FO flux reduction may also be influenced by factors other than fouling, such as the dilution of the DS, which occurs in the AL-FS of an FO membrane [44], the baseline tests

(where foulant was absent) were also performed as a control test. The fouling experiments were conducted by maintaining identical conditions of CFV, pH, and temperature corresponding to the baseline tests. In the presence of a foulant, a water flux decline was observed. This is primarily due to two factors: lower osmotic pressure due to dilution of DS and concentration of FS, and fouling [44]. The extent of fouling could be evaluated by comparing the water flux curve of a fouled membrane to the baseline which had similarly been influenced by dilution of DS and concentration of FS. For every foulant, the length of the tests was 10 h. A physical cleaning test (water flushing) was immediately performed for 30 min with an increased CFV value (as mentioned in section 2.3) prior to repeating a baseline experiment with a reduction to the initial CFV. Subsequently, flux recovery of the membrane was systematically evaluated to check for fouling reversibility, thereby enabling a determination of the critical flux for irreversibility. During the physical cleaning process, the feed was DI water, and the DS channel drained to ensure the absence of permeate flux through the membrane.

2.7. Parameter determination

2.7.1. Water flux

In brief, the water flux was calculated based on the volume changes in the permeate as a function of time (mintue by minute), which was adopted from the prior studies. The equation for water flux is as follows:

$$J_t = \frac{1}{A_m}\frac{\Delta V}{\Delta t} \quad (1)$$

where J_t is the water flux (LMH) at time t, A_m is the effective membrane area (m^2, 0.001875 m^2 in the current study), V is the volume of collected permeate (L), and t is the time for collecting the permeate (h).

2.7.2. Quantification of water flux decline for long-term experiments

To evaluate the water flux decline caused by the effect of dilution or fouling, the percentage of flux decline was considered to access the long-term operation. In the baseline experiment, a water flux decline due to the effect of concentrating the FS and DS dilutions [44], which led to the loss of osmotic driving force across the membrane is presented as follows:

$$\% \text{ flux decline in baseline test} = (1 - J_{wb}/J_{wbo}) \times 100\% \quad (2)$$

where J_{wb}/J_{wbo} is a normalized flux of the baseline experiment; J_{wb} is the final flux of the baseline experiment (LMH); J_{wbo} is the initial flux of baseline experiment (LMH).

Meanwhile, a flux decline was induced simultaneously by the effect of dilution and the occurrence of fouling in the fouling experiment:

$$\% \text{ flux decline in fouling test} = (1 - J_{wf}/J_{wfo}) \times 100\% \quad (3)$$

where J_{wf}/J_{wfo}, is a normalized flux of the fouling experiment; J_{wf} is the final flux of the fouling experiment (LMH); J_{wfo} is the initial flux of the fouling experiment (LMH)

2.7.3. Fouling reversibility

The reversibility of the fouling layer deposited on an active layer was determined using physical cleaning for 30 min with elevated CFV (twice the value used in the fouling experiment). The cleaning effectiveness is shown in the equation below:

$$R\ (\%) = \frac{J_c - J_a}{J_b - J_a} \times 100 \quad (4)$$

where J_a is the water flux after the fouling experiment (LMH); J_b is the water flux before fouling (pristine membrane) (LMH); J_c is the water flux after physical cleaning (LMH).

3. Results and discussion

3.1. Critical flux determination using single foulant

A comparison of the results from the baseline tests with those from single fouling tests is shown in Fig. 2. The DS concentration was gradually increased via stepping from 0.25 M to 3 M with a step interval of 30 min. The results allowed the determination of the critical flux behavior for an FO single foulant. Regarding the baseline experiments, the water flux increased as the DS concentration (and hence the osmotic driving force) was increased. A stable flux was obtained in the baseline tests at various DS concentrations (0.25–2 M) for both the CTA and PA-TFC membranes. However for the 3-M DS, a slight water flux decline was observed under the baseline condition due to the combination of FS concentration and DS dilution; both lead to a loss of osmotic driving force across the membrane [44]. The water flux of PA-TFC is approximately two times higher than that of the CTA membrane, as shown in Fig. 2, despite having the same DS concentration. This is due to the PA-TFC membrane having a lower structural parameter and contact angle, and a much higher 'A' parameter (see Table 2). Subsequently, foulants such as alginate (200 mg/L), colloidal silica (1000 mg/L), and gypsum scaling (20 mM Na_2SO_4 and 20 mM $CaCl_2$) were added singularly into the FS. The variation of water flux upon fouling with single foulants is presented in Fig. 2.

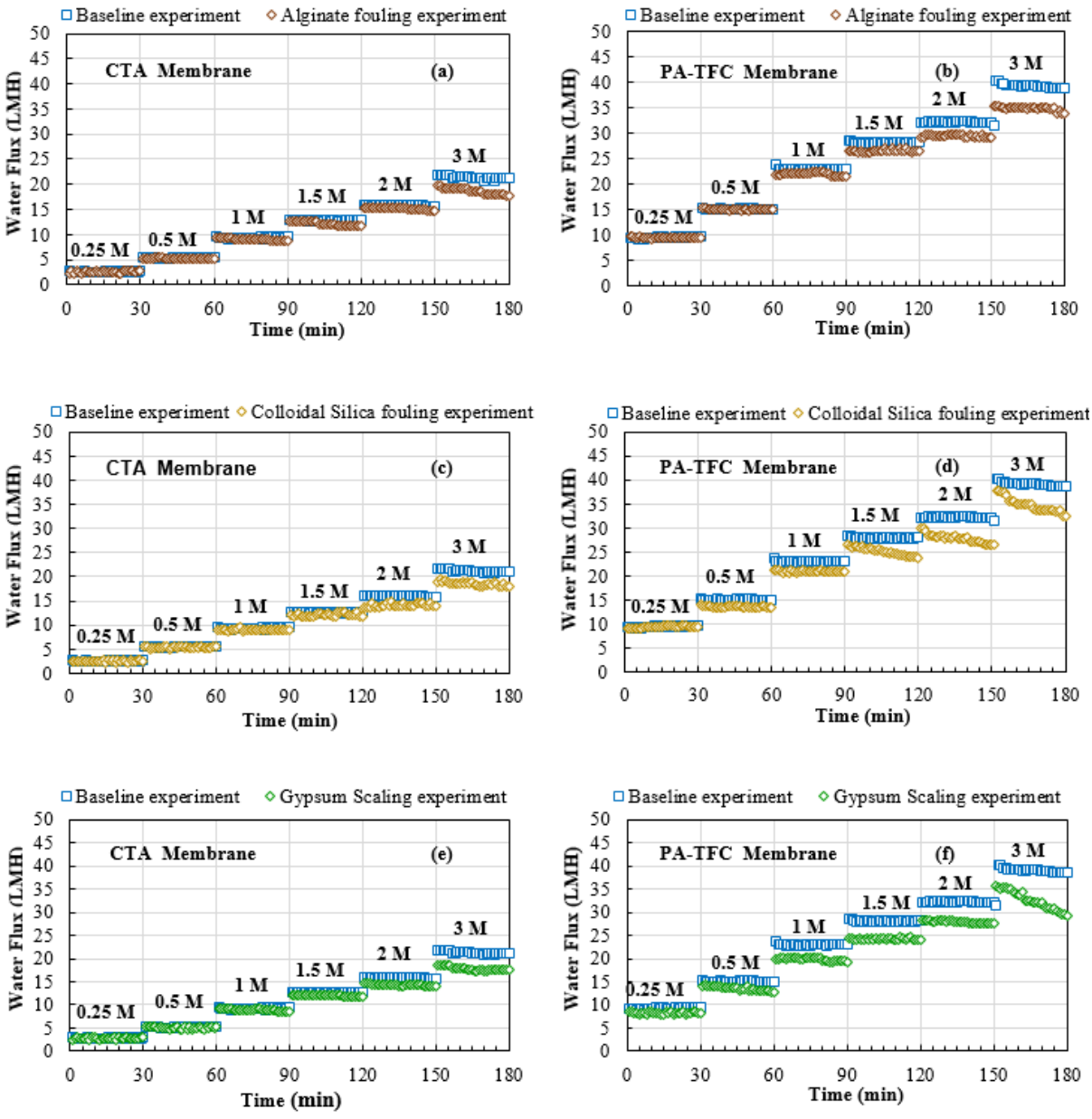

Figure 2. Flux behavior of various single foulants: alginate (a, b), colloidal silica (c, d), gypsum scaling (e, f), for a range of DS-concentrations (0.25–3 M) for the CTA membrane (left) and PA-TFC membrane (right)

The degree of fouling can be evaluated by comparing the water flux curve of a fouled membrane to the baseline. It is noteworthy that the fouling rate at various single fouling scenarios was

gradually promoted as the DS concentration is increased, corresponding to elevated water flux. The increase in membrane fouling with a higher initial fluxcan be primarily attributed to the larger hydrodynamic drag force that enhances the foulant deposition onto the membrane [46] [44] [47]. With respect to alginate fouling (Fig. 2-a, b), the flux curves overlap with the baseline flux curves for DS concentrations of 0.25–1.5 M (flux: 2.7–12.5 LMH), and 0.25–0.5 M (flux: 8.3–12.8 LMH) for the CTA and PA-TFC membranes, respectively. Otherwise, the water flux started deviating from the baseline at higher DS concentrations of 2 M (CTA) and 1 M (PA-TFC), directly indicating a reduction in water flux at these conditions due to the addition of alginate. In some cases the water flux fouling flux did not decline although the initial flux in fouling was lower than that of the baseline. This same trend was observed in a study by Zou et al., [43], who observed foulant deposition onto a membrane using direct microscopic observation.

Fig. 2-c, d, e, f present the fouling trends of colloidal silica and of gypsum scaling with respect to each DS concentration (0.25–3 M). Similarly, an overlap between the fouling flux and baseline flux was observed for DS of 0.25–1.5 M for the CTA membrane, which shows the same trend as alginate fouling. We can assume that the CTA membrane is less sensitive to various single foulants when operating at a low or moderate initial flux. Meanwhile, for the PA-TFC membrane, this overlap only appeared at a low DS of 0.25 M. A deviation from the baseline flux was immediately recorded when operation at 1-M DS was started for both colloidal silica and gypsum scaling. Specifically, a steady upward trend in fouling of the colloidal silica and gypsum was observed with further increases in DS concentration. In particular the PA-TFC membrane was found to be more prone to fouling by a single foulant at an operation of moderate or high initial flux (28.0–39.0 LMH). This agreed with the study of Yu et al. [49], who reported that severe fouling can occur even at moderate flux levels (25 LMH), especially for PA-TFC. Additionally, they reported that

for TFC membranes the surface roughness plays a more dominant role over surface hydrophilicity in membrane fouling [49]. Moreover, membrane surface morphology has been demonstrated as a factor that largely affects the foulant–membrane interaction [48]. Therefore, with a much rougher surface (data in Table 2) and a higher initial flux (Fig. 1), the fouling by a single foulant in the PA-TFC membrane can be more significant, for a given DS concentration, compared to that with the CTA membrane. This result is also consistent with that of Mazlan et al. [30], who indicated a greater adhesion of foulant on the TFC active surface, which could be attributed to factors such as surface roughness, surface charge, surface chemical heterogeneity, and hydrodynamic effects. Finally we note that for the same flux of say 15.0 LMH the rate of fouling was similar for both membranes.

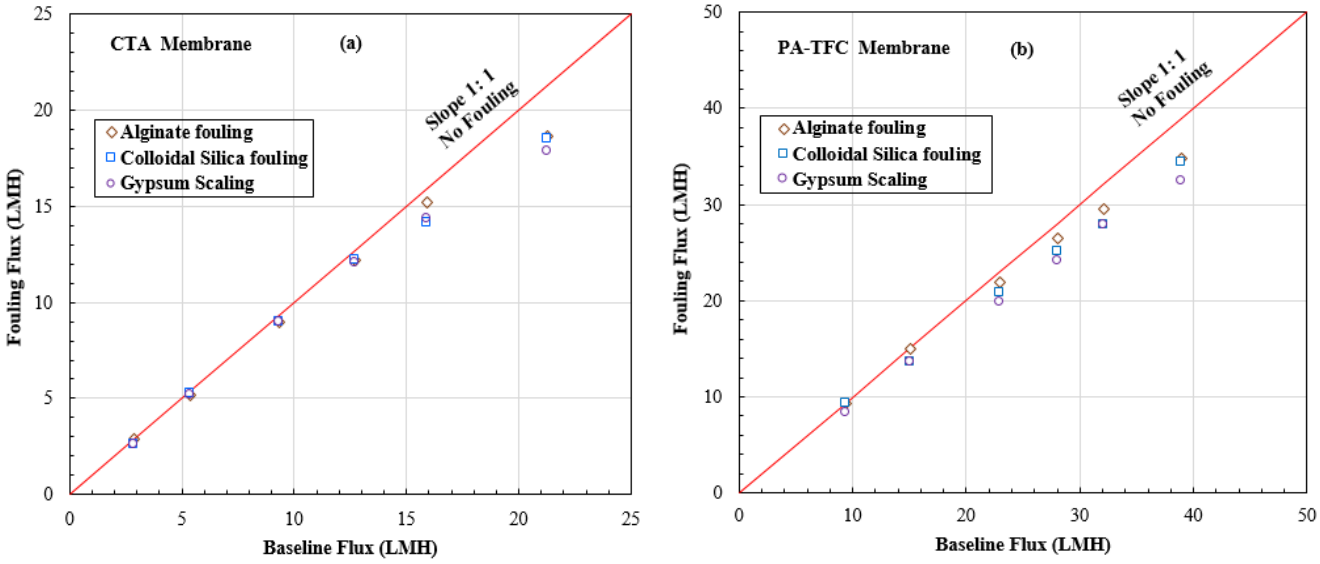

Figure 3. Critical flux behaviors when various single foulants (◊) alginate, (□) colloidal silica, and (○) gypsum scaling) were tested in AL-FS orientation for (a) CTA membrane and (b) PA-TFC membrane. The fouling flux was plotted against the baseline flux, and data points below the line with 1:1 slope indicate the occurrence of flux decline due to fouling.

Based on the flux measurements, a precise determination of the critical flux values was made by plotting the fouling flux (at the end of each DS concentration step) against the corresponding baseline flux (Fig. 3). The line with a 1:1 slope denotes no fouling (i.e., fouling flux equals the corresponding baseline flux). Each foulant type has specific properties (i.e., alginate: transparent gel layer [31], colloidal silica: particulate [26] [50], gypsum: crystallization [51]), thus resulting in various forms of membrane interactions, leading to different fouling potentials on the FO membrane. When the FS contains only a single foulant, a mild fouling condition is induced but with a strong membrane dependence [49]. Membrane surface properties (surface roughness, caused by functional groups bonding) and hydrodynamic conditions (initial flux, cross-flow velocity) have been known to be vital factors for controlling membrane fouling [30]. Therefore, a distinct critical flux behavior between CTA and PA-TFC can be anticipated. As illustrated in Fig. 3-a, the critical flux behavior of the CTA membrane for alginate fouling was found to be within the range of 12.5–15.9 LMH (critical DS 1.5–2 M). A critical flux value of 12.5 LMH (critical DS 1.5 M) was found for both the colloidal silica and gypsum scaling. Regarding PA-TFC, a higher critical flux was found for alginate compared to the other foulants, the value being 20.5 LMH (critical DS 1 M) compared to 12.8 LMH (critical DS 0.5 M). Interestingly, the critical flux values by the single foulants were higher for the PA-TFC membrane compared to those of the CTA membrane although previous studies have reported that PA-TFC has a more pronounced fouling propensity [49] [48] [30]. As noted in [32], the length of experiments can influence the determination of the critical flux values. Thus to refine the determination of critical values, an essential investigation into operational critical fluxes with long-term experiments was performed (in section 3.3.1).

3.2. Critical flux determination using combined foulant

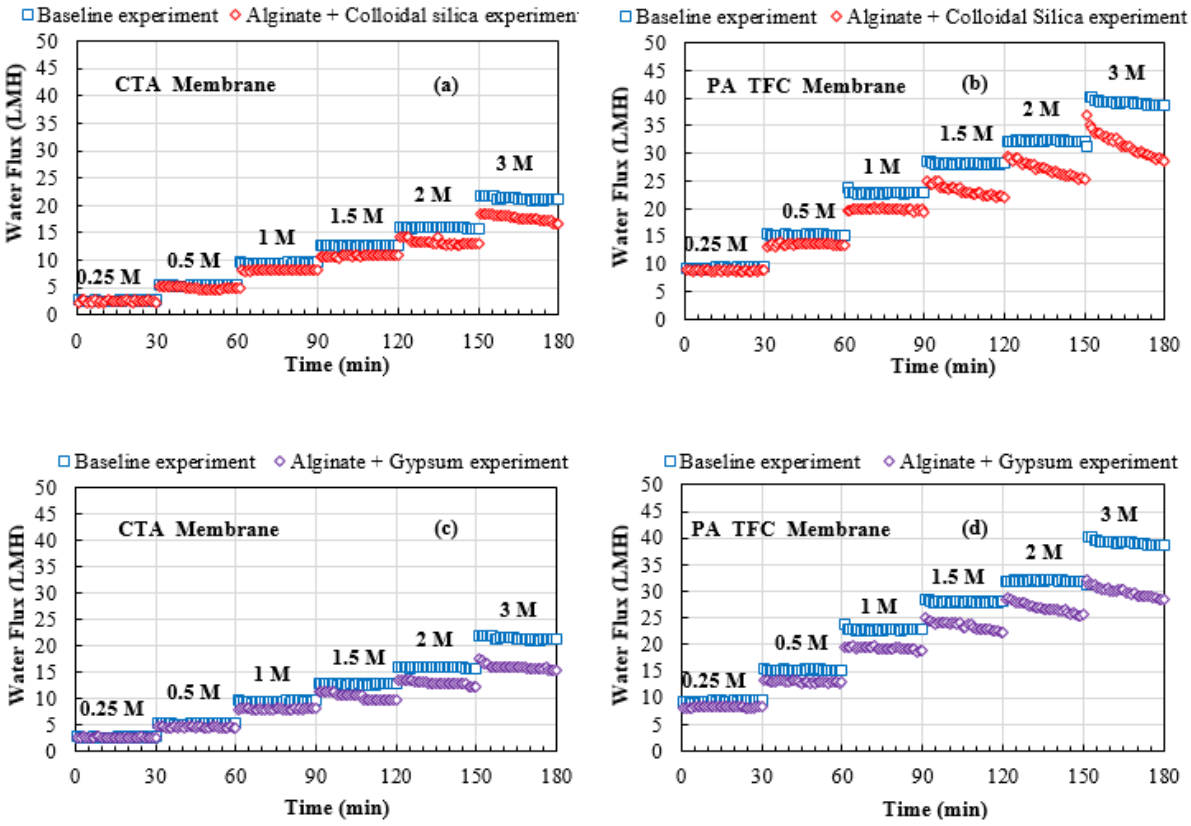

382

383 **Figure 4.** Flux behavior of various combined foulants (a, b) alginate + colloidal silica, (c, d)
384 alginate + gypsum scaling with the DS-concentration step function (0.25–3 M) for CTA membrane
385 (left) and PA-TFC membrane (right)

386

387 In general, various foulant types are present in wastewater and surface water. Therefore an
388 investigation of the critical flux behavior by combined fouling is necessary. Fig. 4 presents the flux
389 behavior of various combined foulants (i.e., alginate + colloidal silica, and alginate + gypsum
390 scaling) as the DS-concentration is increased step wise from 0.25 to 3 M both for CTA membrane
391 (a, c) and PA-TFC membrane (b, d). Regarding the CTA membrane, at low DS concentrations of
392 0.25–0.5 M (corresponding to low flux of 2.7–5.4 LMH), an entire overlap between the fouling
393 flux and baseline flux was observed for the combined foulants (Fig. 4-a, c), indicating negligible
394 fouling. In contrast, at DS concentrations of 1–3 M (flux range 9.0–17.8 LMH), fouling started to

appear as indicated by the fouling flux deviating from the baseline flux. This indicates that for the CTA membrane an effective control of combined fouling can only be achieved at an extremely low initial flux, which might be insufficient for economical application of FO membrane process.

For the PA-TFC membrane, only DS of 0.25 M (corresponding to flux of 9.4 LMH) showed an overlap between the fouling flux and baseline flux (i.e., negligible fouling). When the DS was increased from 0.5 M to 3 M, fluxes in the range 12.8–39.0 LMH were found but there was deviation between the fouling flux and the baseline flux for DS concentration of 0.5 M upwards. The extent of fouling increased steadily with increased DS concentration. From Fig. 4, for each DS concentration it can be observed that clear deviation follows the following order: alginate + gypsum > alginate + colloidal silica. Also PA-TFC > CTA and the reasons for this are primarily due to the higher initial flux [26] [50] [51] and rougher surface of the PA-TFC membrane (Table 2). The finding of a more complex fouling by alginate combined with gypsum accords with those of others [14] [49] [52]. Gu et al. [49] reported that severe fouling for PA-TFC at either moderate flux levels of around 25.0 LMH or with combined foulants. They mentioned that in addition to membrane–foulant interaction, foulant–foulant interaction was important [49]. Moreover and more generally, previous studies have reported that a susceptibility to fouling occurs when the membrane surface becomes covered by fouling [44] [49] [52]. Consequently, further deposition is governed by interaction between the foulant cake layer and foulants in the FS [49].

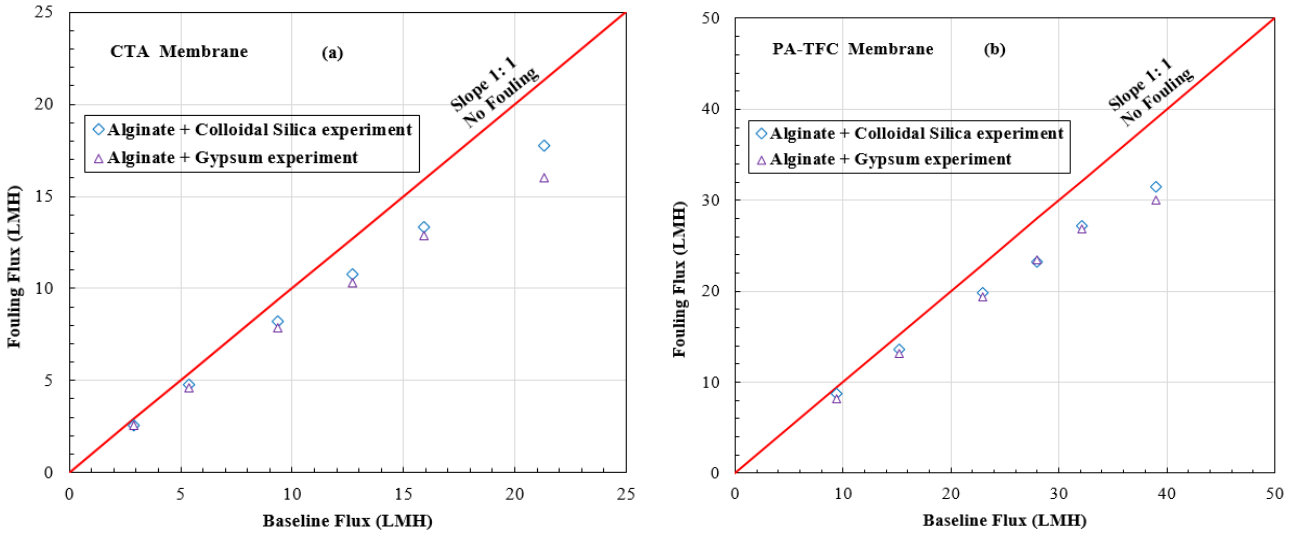

Figure 5. Critical flux behaviors when various combinations of foulants: (◊) alginate + colloidal silica, (Δ) alginate + gypsum scaling were tested in the AL-FS orientation for (a) CTA membrane and (b) PA-TFC membrane. The fouling flux was plotted against the baseline flux, and data points below the line with 1:1 slope indicate the occurrence of flux decline due to fouling.

As illustrated in Fig. 5, the fouling flux is plotted against the corresponding baseline flux to determine the critical flux values for combined foulants. As mentioned above (section 3.1), the potential fouling on an FO membrane was different for each foulant type. However, when more than one type of foulant is present, the interaction among foulants can result in various changes such as physical changes in size and molecular weight and chemical changes e.g. charge and hydrophobicity [53] [41] [51] [52] [54]. Such changes explain the finding that the critical flux for the CTA membrane was just 5.2 LMH (corresponding to DS 0.5 M) for both combined fouling conditions. This value is to be compared to the finding that for single foulants the critical flux was between 12.5 and 15.9 LMH. The determination of the critical flux behavior of PA-TFC membranes under combined fouling conditions found that for alginate combined with colloidal

silica the critical flux was 12.8 LMH (corresponding to DS 0.5 M). Meanwhile, for alginate + gypsum the value is lower than 9.4 LMH (corresponding to DS < 0.25 M). Whilst a short-term test at a lower DS concentration was not performed, a DS concentration of 0.15 M was investigated in long-term test of alginate + gypsum fouling (in section 3.3.2)

3.3. Membrane fouling behavior in long-term tests

3.3.1 Single foulant

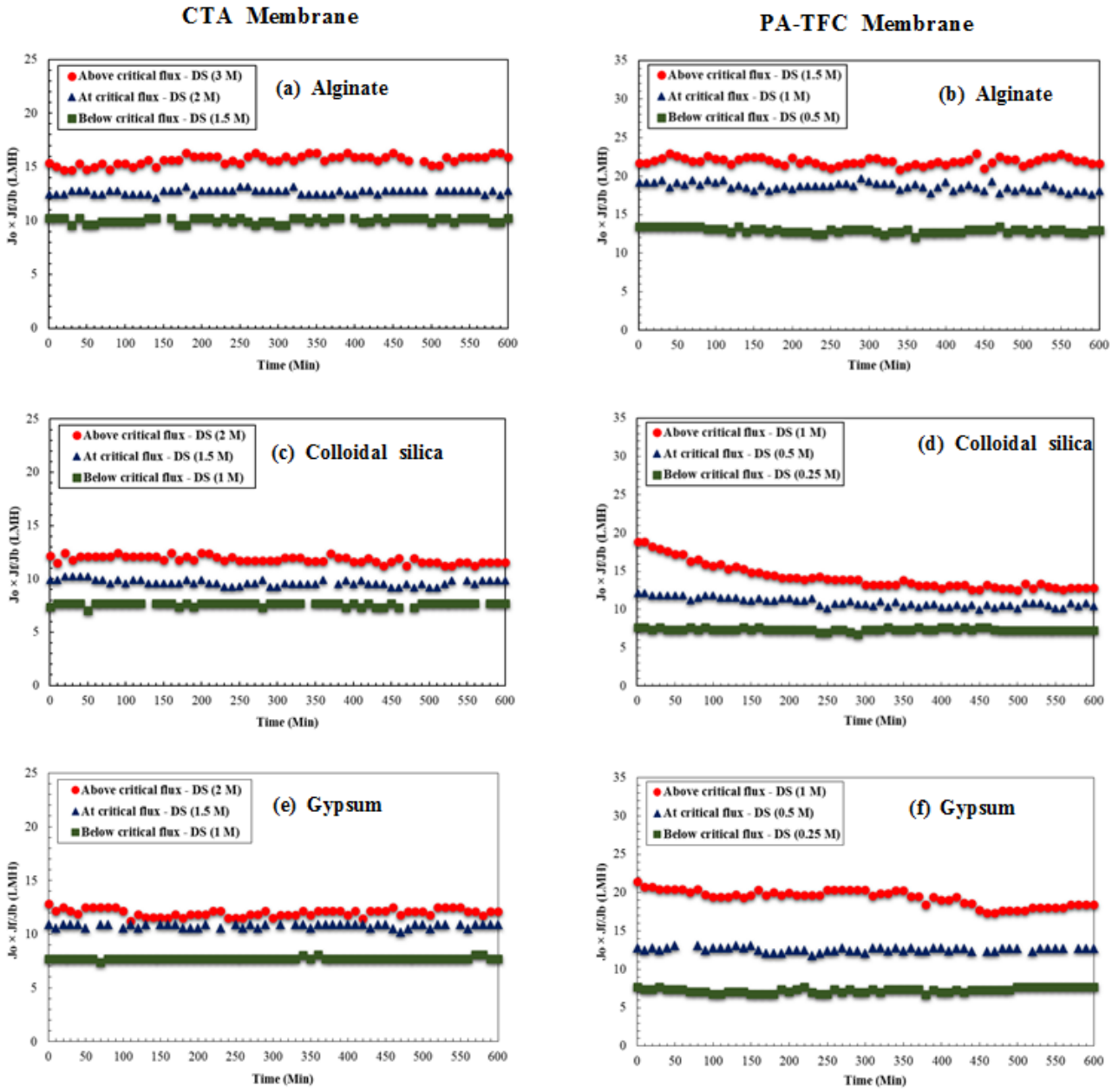

438

439 **Figure 6.** Water flux behavior as a function of time for various single foulants under three
440 operational conditions: above critical flux, at critical flux, and below critical flux. Single fouling
441 experiments:(a, b) alginate, (c, d) colloidal silica, (e, f) gypsum scaling for CTA membrane (left)
442 and PA-TFC membrane (right). J_o x J_f/J_b is a normalized representation of the extent of membrane
443 fouling. J_o represents the initial flux, J_f is the flux in the fouling test, J_b is the baseline flux.

According to the critical flux value obtained in the short-term test (in section 3.1), a long-term experiment of 10 h was performed to not only investigate the reliability of the DS concentration stepping method but also to determine the influence of the fluxes around these critical values on the fouling behavior. Fig. 6 shows the water flux decline as a function of time at various single foulants under operational critical fluxes (above critical flux, at critical flux, below critical flux). The desired DS concentration was changed based on the design shown in Table S-1. In the baseline experiments for both membranes (Fig. S-2), water flux flows from the feed to the draw side, inherently induces a simultaneous concentration of feed and dilution of the draw. A higher water flux reduction was caused by the larger dilution [44], which became severe in the PA-TFC membrane because of higher flux. For the CTA membrane, by comparing the water flux curve of a fouled membrane to the baseline (J_o x J_f/J_b is a normalized representation of the extent of membrane fouling), the extent of fouling could be evaluated for the various single foulants such as alginate, colloidal, and gypsum (Fig. 6- a, c, e and Fig S-2-a, c, e). An unstable flux (Fig. 6) and a flux reduction caused by fouling (Fig S-4) was observed above the critical flux, i.e., 3-M DS (alginate), 2-M DS (colloidal silica), 2-M DS (gypsum), whereas negligible or even no fouling occurred at the critical flux and below it. When operating below the critical flux, the flux decline appears to result only from the effect of draw dilution (Fig. S-4), which indicates less sensitivity to single fouling of the CTA membrane (as stated in section 3.1). These findings suggest the existence of critical fluxes (J_{crit}) for single foulants and the CTA membrane as follows: $J_{crit} \approx 15.9$ LMH (alginate), $J_{crit} \approx 12.5$ LMH (colloidal silica), $J_{crit} \approx 12.5$ LMH (gypsum). Obviously, a sustainable operation without fouling could be achieved by setting an appropriate flux (i.e., close to or below critical flux); this promotes the minimization of fouling of the CTA membrane by single foulants.

Regarding the PA-TFC membrane (Fig. 6-b, d, f and Fig S-2, b, d, f), fouling occurred above the critical flux being considerable for colloidal silica, moderate for gypsum and slight for alginate, with all being much greater compared to that with the CTA membrane. As mentioned in sections 3.1 and 3.2, either a high initial flux or the properties of the membrane surface (i.e., much rougher, bonding of functional groups) was the primary reason of vulnerable fouling in the PA-TFC membrane. This finding accords with others for instance, Mi et al. [55] demonstrated that surface roughness caused an increase in the adhesion force between the PA-TFC membrane and a colloidal silica gel layer. Kim et al. [56] also concluded that the structure of colloidal fouling was significantly dependent on the initial permeate flux, with the fouling transitioning from fluid-like to solid-like [57], thereby promoting excessive fouling [51]. According to previous studies, severe fouling with colloidal silica is to be expected and for the resultant flux decline to be magnified by the effect of cake enhanced-concentration polarization (CE-CP), thereby significantly increasing the overall FO flux decline [42] [26] [50] [28]. Meanwhile, gypsum scaling was accelerated because of a greater membrane surface roughness [58] [59] and the rich presence of the carboxylic group (-COO-), which could interact with the Ca^{2+} ions to form a complex foulant [51] [59]. Additionally, the role of the initial flux was also pronounced in the gypsum scaling behavior, i.e., more than 50% water flux decline was recorded when the initial flux was increased from 10 LMH to 25 LMH with PA-TFC [51]. Other previous studies have indicated that a dominant heterogeneous crystallization occurs in gypsum scaling on PA-TFC, thus causing a much larger degree of fouling than that with a CTA membrane [51] [29]. Fig. 6 and Fig. S-4 show that the considerable flux decrease via fouling began to appear with colloidal silica foulant, when operating above the critical flux condition. Contrastingly just a minor degree of fouling and a sustainable flux were observed close to or below the critical values. When there is an acceptable minor degree of fouling it has been suggested that the term threshold flux be used and it can be defined as the flux

491 at or below which low fouling occurs but above which the fouling rate increases significantly [25].
492 However this distinction is not made here. With single foulants and the PA-TFC membrane,
493 operation is super-critical at a higher flux of 20.0 LMH, but fouling control could be successfully
494 achieved by operation at the following values: J_{crit} ≈20.5 LMH (alginate), J_{crit} ≈ 12.8 LMH
495 (colloidal silica), J_{crit} ≈ 12.8 LMH (gypsum).
496
497 **3.3.2 Combined foulant**
498 Fig. 7 depicts the water flux behavior as a function of time for various combined foulants under at
499 fluxes above critical flux, at critical flux, and below critical flux. The corresponding DS
500 concentrations are given in Table S-1. As discussed in section 3.2, the presence of colloidal silica
501 or gypsum partially contributed to the formation of a complex foulant layer, causing a more severe
502 fouling. For example, the study of Motsa et al. [41] demonstrated that the significant flux loss of
503 the CTA membrane in combined fouling (i.e., alginate + colloidal silica) was due to the hydraulic
504 resistance of a gel layer that hindered back diffusion of the colloid and gave rise to CE-CP. Their
505 experiments were operated with an initial flux of 15.8 LMH (i.e., DS 3.5 M). In addition, the
506 synergistic effect of combined fouling (i.e., alginate + gypsum) was investigated at an initial flux
507 of 17.6 LMH (DS 4 M), in which accelerated gypsum scaling due to CE-CP has been reported for
508 a CTA membrane [14]. Liu et al. [52] found that alginate molecules could act as nuclei for gypsum
509 crystal growth, thus considerably increasing the gypsum crystal size and aggravating their
510 deposition onto a CTA membrane; their experiments were operated with an initial flux of 16.2
511 LMH. However, in the current study with the CTA membrane, combined fouling (i.e., alginate +
512 gypsum) only a slight flux decline above the critical flux was observed. This is due to a lower initial
513 flux (operation was at 9.0 LMH corresponding to DS 1 M) and a lower Ca^{2+} concentration (i.e.,
514 20-mM Na_2SO_4 and 20-mM $CaCl_2$ was used in this study). In previous studies the initial fluxes

were 16.2–17.6 LMH and Ca^{2+} concentration was higher owing to the use of 20-mM Na_2SO_4 and 35-mM $CaCl_2$ [14] [52]**.** Meanwhile in the present study sustainable fluxes were found at the critical flux and below the critical flux (i.e., DS 0.5 M and DS 0.25 M) (Fig. 7-a, c). Clearly with respect to the CTA membrane, control of combined fouling can be achieved by selection of an appropriate DS concentration; a lower DS concentration gives a lower initial flux.

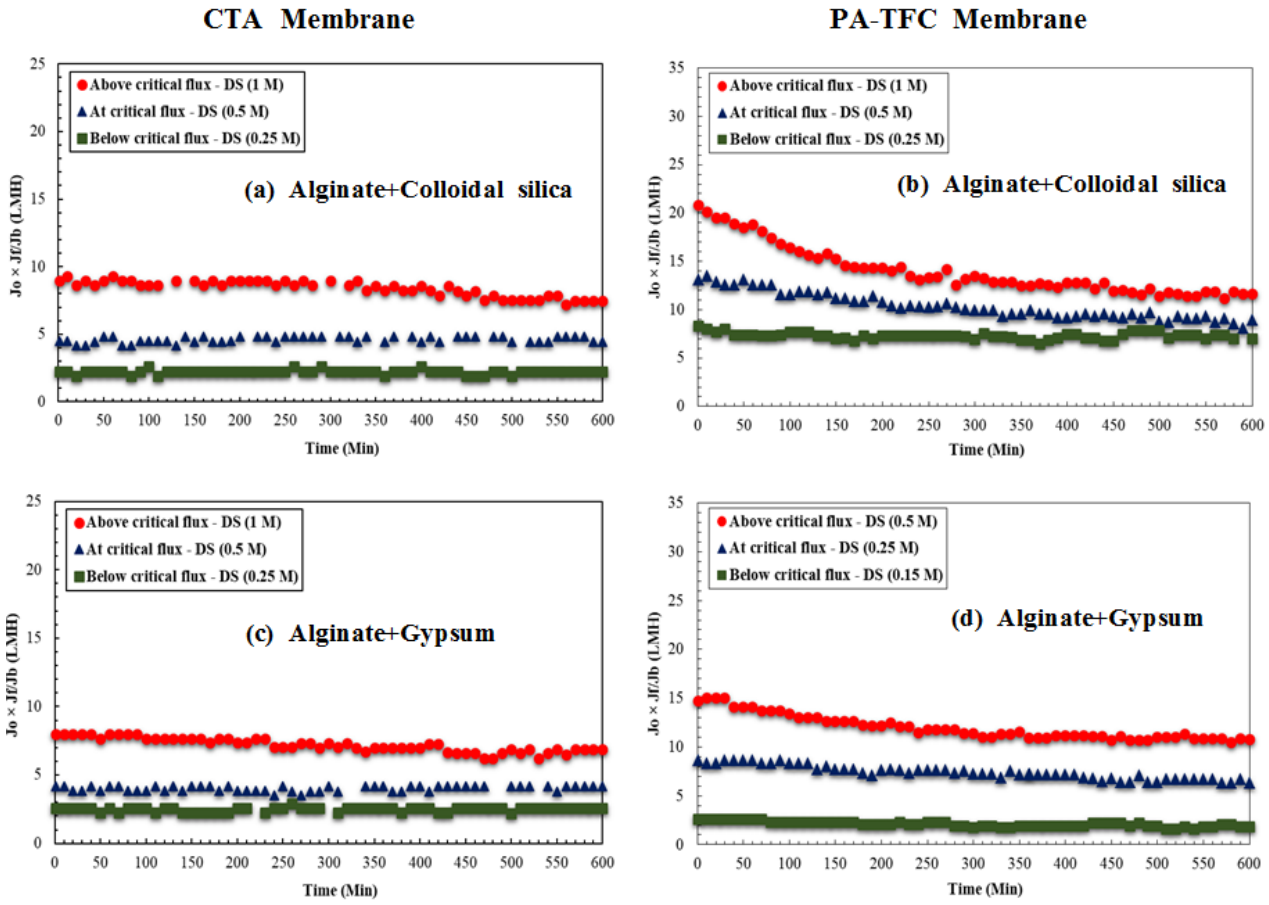

Figure 7. Water flux behavior as a function of time for combined foulants under three operational conditions: above critical flux, at critical flux, and below critical flux. (a, b) alginate + colloidal silica, (c, d) alginate + gypsum scaling for CTA membrane (left) and PA-TFC membrane (right). J_o *x* J_f/J_b is a normalized representation of the extent of membrane fouling. J_o represents the initial flux, J_f is the flux in the fouling test and J_b is the flux in the baseline test.

Above the critical flux the water flux declined dramatically after 10 h of operation, indicating significant fouling (Fig. 7-b, d and Fig S-3-b, d). However, a negligible fouling of PA-TFC was observed below the critical flux for both combinations of mixed foulants, resulting in a sustainable flux. The critical flux values for the combined foulants were different being $J_{crit} \approx 12.8$ LMH for alginate + colloidal silica and $J_{crit} \approx 8.3$ LMH for alginate + gypsum. Clearly, for the PA-TFC membrane fouling control with alginate + gypsum is more difficult than that of alginate with colloidal silica. As discussed in section 3.1, for single gypsum fouling, the presence of a rich carboxylic group (-COO-) in PA-TFC [37] could interact with the Ca^{2+} ions to generate a homogeneous crystallization [52]; this being an example of adverse membrane–foulant interaction. Moreover, this fouling becomes more severe in the presence of alginate (i.e., a large number of negatively charged carboxylate (-COO-)). A more complex matrix with the calcium ion of gypsum is created which increases the crystal size[14]; this being an example of adverse foulant–foulant interaction. A summary of critical flux values is given in Table 4.

Table 4. Critical flux values for fouling (LMH)

Foulants	**Critical Flux for fouling (J_{crit})**	
	CTA	**PA-TFC**

Single foulant		
Alginate	15.9	20.5
Colloidal silica	12.5	12.8
Gypsum	12.5	12.8
Combined foulants		
Alginate + gypsum	5.4	8.3
Alginate + colloidal silica	5.4	12.8

Note: The critical values above are specific for the FO membrane process with the conditions: i) FO mode (AL-FS), ii) Feed and draw flow rate of 300 mL/min (equivalent CFV of 6.66 cm/s), iii) Foulant concentration: 200 mg/L alginate, 1000 mg/L colloidal silica, gypsum scaling (20 mM Na_2SO_4 and 20 mM $CaCl_2$) and iv) determination after flux stepping with a step interval of 30mins.

3.3.3 Fouling reversibility and critical flux for reversibility

Distinguishing between reversible and irreversible fouling is a vital to a proper assessment of the fouling propensity of a FO membrane as well as to the potential recovery of water flux. Therefore, in the current study when fouling had occurred, membrane flushing was performed for 30 min after the fouling test to assess the degree of fouling reversibility . The results enabled us to establish the critical flux for reversibility (J_{ci}). Fig. 8 shows the water flux recovered after the physical cleaning of membranes fouled in the single foulant studies; there aresome blanks were the test was not performed because there had been no fouling. In detail, the normalized flux after fouling showed an increasing trend as the DS concentration decreased (i.e., lower initial flux), for both membranes and three single foulants. As discussed in section 3.1, factors such as the initial flux, foulant type, and membrane type led to a different impact on the membrane fouling propensity.

566 Regarding alginate fouling (Fig. 8-a), PA-TFC showed a higher fouling rate than the CTA
567 membrane above critical flux conditions because of a higher initial flux. Nevertheless, we noticed
568 that the flux recovered by physical cleaning appear to be the same for both membranes, with
569 recoveries of 95%. It is likely that the fouling by alginate could be readily reversible, which was
570 successfully demonstrated in previous studies with the CTA membrane [14] [31] [26] [27] and PA-
571 TFC membrane [11]. Interestingly, 98-100% recovery of water flux was recorded at close to and
572 below the critical flux i.e. 12.8 LMH (DS 0.5 M) for the PA-TFC membrane and at above critical
573 flux i.e. 15.9 LMH (DS 3 M) for CTA membrane; thus, they do accord with the critical flux for
574 reversibility [32]. As stated in section 3.1, although PA-TFC still exhibited a slight fouling with
575 alginate below the critical flux (Fig. S-4, b), this fouling could be completely restored (Fig. 7-a).
576 Obviously, an appropriate operation (i.e., close to or below critical flux) could help minimize the
577 alginate fouling of PA-TFC membranes and promote fouling reversibility. A lower DS
578 concentration was set to meet the operational critical flux conditions in colloidal silica fouling (Fig.
579 8-b). As mentioned in section 3.3.1, in operation above the critical flux, colloidal silica showed a
580 more noticeable fouling tendency than alginate despite operation being at a lower initial flux (lower
581 DS concentration) (Fig. 6). This was particularly noticeable with the PA-TFC membrane, which
582 reached a low normalized flux of 0.55 after the formation of the fouling layer (Fig. 7-b). In addition,
583 a low cleaning effectiveness was found for PA-TFC (i.e., 50%) indicating that with colloidal silica
584 fouling this membrane gave poor recovery when starting above the critical flux (i.e., 20.5 LMH).
585 This trend is consistent with the study of Xie et al. [53], who showed the effect of initial flux on
586 the recovery of a TFC membrane subject to colloidal fouling (e.g., a flux of 20 LMH corresponded
587 to a low recovery of 30%). However, for both membranes, a better recovery after colloidal silica
588 fouling was obtained after operation at critical flux i.e. at 12.5 LMH (CTA) and 12.8 LMH (PA-
589 TFC), and below critical flux condition i.e. at 8.3 LMH (PA-TFC). For the former and latter, high

values of 94% and 100% recovery respectively were found (Fig. 7-b). The study of Mi et al. [55] indicated that the surface roughness of PA-TFC played an important role in increasing the membrane–silica interaction, thus significantly decreasing the water flux recovery. However, in this study, it is noteworthy that PA-TFC exhibited a completely reversible fouling (roughly 100% recovery) when operating below the critical flux i.e., at 8.3 LMH (DS 0.25 M). Regarding gypsum scaling, it can be remarked that the physical cleaning appears to be more efficient after gypsum fouling of the CTA membrane with a high value of 97% recovery for operation above critical flux i.e. 15.9 LMH (DS 2.0 M). For the PA-TFC membrane similar recovery (98%) was found at the critical flux condition i.e. 12.8 LMH (DS 0.5 M). In summary, after fouling with single foulants membrane permeability could be well recovered by simple physical cleaning. Consequently this mode may offer the extraordinary advantage of significantly reducing or even eliminating chemical cleaning. The concept of critical flux for reversibility (J_{ci}) was defined by Bachin et al. [34] as "the permeate flux above which a multi-layer of irreversible fouling occurs". This accords with the results above and thus shows the existence of a critical flux for reversibility for both FO membranes tested. The J_{ci} results for the CTA and PA-TFC membranes are summarised in Table 5.

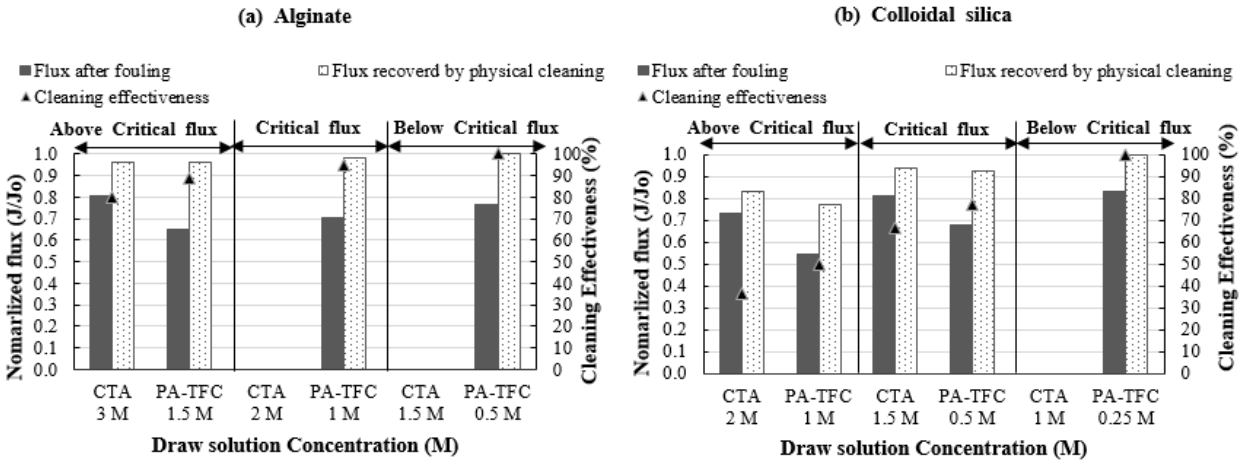

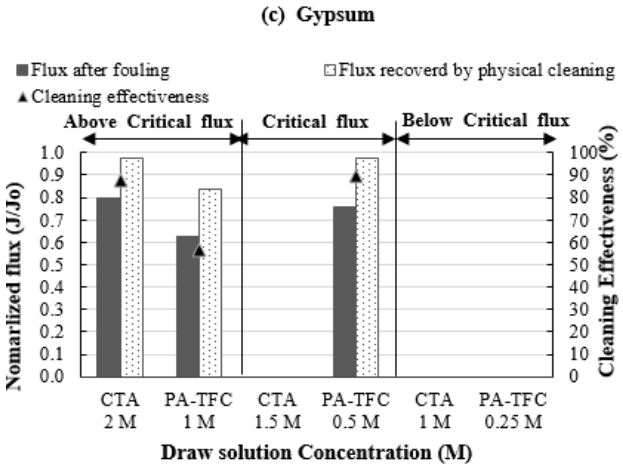

Figure 8. Water flux recovery after physical cleaning of membranes fouled by various single foulants: (a) alginate, (b) colloidal silica, (c) gypsum scaling at various operational fluxes (above critical flux, critical flux, below critical flux). Flux recovery was calculated from water permeability measuremnts taken between 15 min and 30 min after the physical cleaning step. Blanks exist where no fouling was observed during the fouling tests. (Alginate: CTA- DS 2M (at critical flux), 1.5 M (below critical flux); Colloidal silica: CTA-DS 1M (below critical flux); Gypsum: CTA- DS 1.5M (at critical flux), 1M (below critical flux) and PA-TFC- DS 0.25 M (below critical flux)).

An investigation of fouling reversibility by combined foulants is presented in Fig. 9. With the PA-TFC membrane both combined foulants caused significant decline in water flux over 10 h of operation for all conditions used (Fig. 8-a, b). In contrast the CTA membrane showed no flux decline over 10 h of operation in half of the cases. For the others a moderate reduction in water flux occurred with the normalized flux being 0.71 (above critical flux) and 0.8 (at critical flux) for alginate + colloidal silica, and 0.73 (above critical flux) for alginate + gypsum. The lower susceptibility of the CTA membrane to fouling is attributed, in part, to the relatively lower initial flux. Additionally the cleaning process depends on various factors such as the foulant-foulant

interaction and foulant-membrane interaction which is influenced by surface roughness, hydrophilicity and bonding to functional groups [60]. Regarding the CTA membrane, Liu et al. [8] reported that after combined fouling by alginate + gypsum the water flux only recovered to approximately 80%; their experiments were operated at a flux of 17.6 LMH (DS 4 M) with 20 Na_2SO_4 mM and 35 $CaCl_2$ mM. However, in the current study, with 20 Na_2SO_4 mM and 20 $CaCl_2$ mM (e.g., gypsum scaling)and at a lower flux of 9.0 LMH (DS 1 M) the CTA membrane exhibited a high water flux recovery of 93%. This shows that the initial flux and concentration of Ca^{2+} ions are critical in determining flux recovery for this combined foulant.

Another one, Kim et al. [27] observed that fouling reversibility with alginate + colloidal silica was only 93% compared to complete flux recovery (i.e., 100%) for single foulants. Their operations were at identical initial fluxes of 25.3 LMH (DS 5 M) with IS =50 mM and pH=7. Meanwhile, the current study indicated that full restoration of water flux was obtained when operating close to critical flux i.e. at 5.4 LMH (DS 0.5 M). From the results (Fig 9), the critical flux for reversibility for the CTA membrane could also be identified. A summary is given in Table 5.

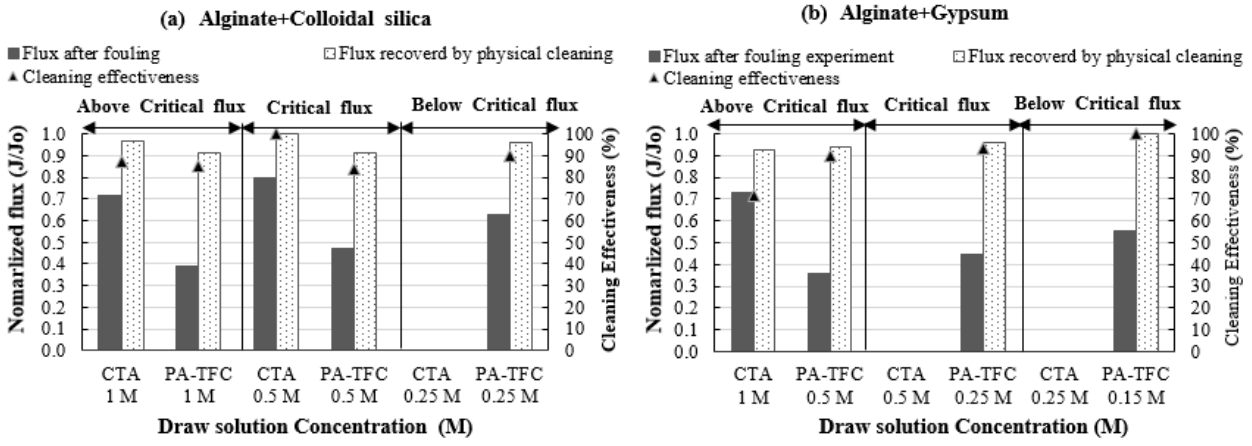

Figure 9. Water flux recovery after physical cleaning of membranes fouled by various combined foulants: (a) alginate + colloidal silica, (b) alginate + gypsum scaling under operational critical flux (above critical flux, critical flux, below critical flux). Water permeating between 15 min and 30

644 min after the physical cleaning step is used for the calculation of flux recovery. Blanks exist where
645 no fouling was observed during the fouling tests.
646
647 As shown in Fig. 9-a, b the results for the PA-TFC membrane are significantly different with the
648 water flux declining after 10 h to normalized fluxes of *circa* 0.6. After combined fouling by alginate
649 + colloidal silica full reversibility was not exhibited with the water flux recovery being around 96%
650 at operation below the supposed critical flux i.e. at 8.3 LMH (DS 0.25 M) and approximately 92%
651 for operation at the supposed critical flux i.e. at 12.8 LMH (DS 0.5 M). For the other combined
652 foulants, 100% recovery was found at operation below critical flux values of 2.3 LMH (DS 0.15
653 M). For the PA-TFC membrane, the complete set of critical flux for reversibility is summarized in
654 Table 5.
655
656
657 **Table 5.** Critical flux values for fouling reversibility (LMH)

Foulants	**Critical Flux for fouling reversibility (J_{ci})**	
	CTA	**PA-TFC**
Single foulant		
Alginate	< 15.9	12.8
Colloidal silica	< 12.5	8.3
Gypsum	< 15.9	< 12.8
Combined foulants		
Alginate + gypsum	< 9.0	2.3
Alginate + colloidal silica	5.4	< 8.3

Note: The values above are specific for the FO membrane process with the conditions: i) FO mode (AL-FS), ii) Feed and draw flow rate of 300 mL/min (equivalent CFV of 6.66 cm/s), iii) Foulant concentration: 200 mg/L alginate, 1000 mg/L colloidal silica, gypsum scaling (20 mM Na_2SO_4 and 20 mM $CaCl_2$), and iv) determination after fouling for 10 h followed by evaluation of fouling reversibility after a 30 min physical clean.

4. Conclusions

First, the existence of critical fluxes in an FO process (CTA and PA-TFC membranes with three single separate foulants) was demonstrated through a reliable stepping method (DS concentration stepping) in conjunction with water flux measurements in short-term experiments. The critical flux behavior in the FO processes was evidently affected by the foulant type and the membrane type. PA-TFC membrane outperformed the CTA membrane in terms of critical flux, which suggests that the former might be favored for practical applications. The critical flux values determined by flux stepping ranged from 5.4 to 20.5 LMH (dependent upon membrane-foulant combination) and these would be adequate for applications in certain FO processes. Finally, 98-100% restoration of water flux was achieved with the PA-TFC membrane at an operation either close to critical flux or below critical flux (i.e., with negligible irreversible fouling), except for the combination of alginate and colloidal silica. This study has confirmed that plant operation below the critical flux (which has also been referred to as sustainable flux or sub-critical operation) is vital for the minimization of chemical cleaning.

Acknowledgment

This research was supported by a grant (code 18IFIP-B087389-05) from the Plant Research Program funded by the Ministry of Land, Infrastructure, and Transport. RWF has been partially

supported by an APEX award (AX170010) granted by a partnership between the Royal Society, the British Academy and the Royal Academy of Engineering. This APEX award is for work on Exploring Water Re-use – the Nexus of Politics, Technology and Economics.

Appendix A: Supplementary data

References

[1] T.Y. Cath, A.E. Childress, M. Elimelech, Forward osmosis: Principles, applications, and recent developments, J. Memb. Sci. 281 (2006) 70–87. doi:10.1016/j.memsci.2006.05.048.

[2] C. Boo, M. Elimelech, S. Hong, Fouling control in a forward osmosis process integrating seawater desalination and wastewater reclamation, J. Memb. Sci. (2013). doi:10.1016/j.memsci.2013.05.004.

[3] T.Y. Cath, N.T. Hancock, C.D. Lundin, C. Hoppe-Jones, J.E. Drewes, A multi-barrier osmotic dilution process for simultaneous desalination and purification of impaired water, J. Memb. Sci. (2010). doi:10.1016/j.memsci.2010.06.056.

[4] M.M. Motsa, B.B. Mamba, A.R.D. Verliefde, Forward osmosis membrane performance during simulated wastewater reclamation: Fouling mechanisms and fouling layer properties, J. Water Process Eng. 23 (2018) 109–118. doi:10.1016/j.jwpe.2018.03.007.

[5] F. Volpin, E. Fons, L. Chekli, J.E. Kim, A. Jang, H.K. Shon, Hybrid forward osmosis-reverse osmosis for wastewater reuse and seawater desalination: Understanding the optimal feed solution to minimise fouling, Process Saf. Environ. Prot. 117 (2018) 523–532. doi:10.1016/j.psep.2018.05.006.

[6] L. Chekli, S. Phuntsho, J.E. Kim, J. Kim, J.Y. Choi, J.S. Choi, S. Kim, J.H. Kim, S. Hong,

706 J. Sohn, H.K. Shon, A comprehensive review of hybrid forward osmosis systems:
707 Performance, applications and future prospects, J. Memb. Sci. (2016).
708 doi:10.1016/j.memsci.2015.09.041.
709 [7] G. Blandin, A.R.D. Verliefde, J. Comas, I. Rodriguez-Roda, P. Le-Clech, Efficiently
710 combining water reuse and desalination through forward osmosis-reverse osmosis (FO-
711 RO) hybrids: A critical review, Membranes (Basel). (2016).
712 doi:10.3390/membranes6030037.
713 [8] A.J. Ansari, F.I. Hai, W.E. Price, J.E. Drewes, L.D. Nghiem, Forward osmosis as a
714 platform for resource recovery from municipal wastewater - A critical assessment of the
715 literature, J. Memb. Sci. 529 (2017) 195–206. doi:10.1016/j.memsci.2017.01.054.
716 [9] A.J. Ansari, F.I. Hai, W. Guo, H.H. Ngo, W.E. Price, L.D. Nghiem, Factors governing the
717 pre-concentration of wastewater using forward osmosis for subsequent resource recovery,
718 Sci. Total Environ. 566–567 (2016) 559–566. doi:10.1016/j.scitotenv.2016.05.139.
719 [10] Q. She, R. Wang, A.G. Fane, C.Y. Tang, Membrane fouling in osmotically driven
720 membrane processes: A review, J. Memb. Sci. 499 (2016) 201–233.
721 doi:10.1016/j.memsci.2015.10.040.
722 [11] M. Xie, J. Lee, L.D. Nghiem, M. Elimelech, Role of pressure in organic fouling in forward
723 osmosis and reverse osmosis, J. Memb. Sci. 493 (2015) 748–754.
724 doi:10.1016/j.memsci.2015.07.033.
725 [12] W.C.L. Lay, T.H. Chong, C.Y. Tang, A.G. Fane, J. Zhang, Y. Liu, Fouling propensity of
726 forward osmosis: Investigation of the slower flux decline phenomenon, Water Sci.
727 Technol. 61 (2010) 927–936. doi:10.2166/wst.2010.835.
728 [13] A.G. Fane, T.H. Chong, J. Zhang, W.C.L. Lay, The Effect of Flux and Pressure on Fouling
729 in Reverse Osmosis Desalination, Proceedings IDA World Congress, (2009) Paper DB09-

128.

[14] Y. Liu, B. Mi, Combined fouling of forward osmosis membranes: Synergistic foulant interaction and direct observation of fouling layer formation, J. Memb. Sci. 407–408 (2012) 136–144. doi:10.1016/j.memsci.2012.03.028.

[15] R.W. Field, D. Wu, J.A. Howell, B.B. Gupta, Critical flux concept for microfiltration fouling, J. Memb. Sci. 100 (1995) 259–272. doi:10.1016/0376-7388(94)00265-Z.

[16] J.A. Howell, Sub-critical flux operation of microfiltration, J. Memb. Sci. 107 (1995) 165–171. doi:10.1016/0376-7388(95)00114-R.

[17] P. Bacchin, P. Aimar, V. Sanchez, Model for colloidal fouling of membranes, AIChE J. 41 (1995) 368–376. doi:10.1002/aic.690410218.

[18] F. Wicaksana, A.G. Fane, P. Pongpairoj, R. Field, Microfiltration of algae (Chlorella sorokiniana): Critical flux, fouling and transmission, J. Memb. Sci. 387–388 (2012) 83–92. doi:10.1016/j.memsci.2011.10.013.

[19] J. Xu, L.G. Ruan, X. Wang, Y.Y. Jiang, L.X. Gao, J.C. Gao, Ultrafiltration as pretreatment of seawater desalination: Critical flux, rejection and resistance analysis, Sep. Purif. Technol. 85 (2012) 45–53. doi:10.1016/j.seppur.2011.09.038.

[20] L. Qi, X. Zheng, G. Li, Factors influencing critical flux of UF membrane in drinking water treatment, Desalin. Water Treat. 56 (2015) 3305–3312. doi:10.1080/19443994.2014.968879.

[21] M. Stoller, Effective fouling inhibition by critical flux based optimization methods on a NF membrane module for olive mill wastewater treatment, Chem. Eng. J. 168 (2011) 1140–1148. doi:10.1016/j.cej.2011.01.098.

[22] Y. Lan, K. Groenen-Serrano, C. Coetsier, C. Causserand, Fouling control using critical, threshold and limiting fluxes concepts for cross-flow NF of a complex matrix: Membrane

754 BioReactor effluent, J. Memb. Sci. 524 (2017) 288–298.
755 doi:10.1016/j.memsci.2016.11.001.
756 [23] T.H. Chong, F.S. Wong, A.G. Fane, Implications of critical flux and cake enhanced
757 osmotic pressure (CEOP) on colloidal fouling in reverse osmosis: Experimental
758 observations, J. Memb. Sci. 314 (2008) 101–111. doi:10.1016/j.memsci.2008.01.030.
759 [24] C.Y. Tang, Y.N. Kwon, J.O. Leckie, Fouling of reverse osmosis and nanofiltration
760 membranes by humic acid-Effects of solution composition and hydrodynamic conditions,
761 J. Memb. Sci. 290 (2007) 86–94. doi:10.1016/j.memsci.2006.12.017.
762 [25] R.W. Field, G.K. Pearce, Critical, sustainable and threshold fluxes for membrane filtration
763 with water industry applications, Adv. Colloid Interface Sci. 164 (2011) 38–44.
764 doi:10.1016/j.cis.2010.12.008.
765 [26] Y. Jang, H. Cho, Y. Shin, Y. Choi, S. Lee, J. Koo, Comparison of fouling propensity and
766 physical cleaning effect in forward osmosis, reverse osmosis, and membrane distillation,
767 Desalin. Water Treat. 3994 (2016) 1–10. doi:10.1080/19443994.2016.1152650.
768 [27] Y. Kim, M. Elimelech, H.K. Shon, S. Hong, Combined organic and colloidal fouling in
769 forward osmosis: Fouling reversibility and the role of applied pressure, J. Memb. Sci. 460
770 (2014) 206–212. doi:10.1016/j.memsci.2014.02.038.
771 [28] Y.N. Wang, E. Järvelä, J. Wei, M. Zhang, H. Kyllönen, R. Wang, C.Y. Tang, Gypsum
772 scaling and membrane integrity of osmotically driven membranes: The effect of membrane
773 materials and operating conditions, Desalination. 377 (2016) 1–10.
774 doi:10.1016/j.desal.2015.08.024.
775 [29] M. Elimelech, Gypsum Scaling and Cleaning in Forward Osmosis : Measurements and
776 Mechanisms, Environ. Sci. Technol. 44 (2010) 2022–2028.
777 [30] N.M. Mazlan, P. Marchetti, H.A. Maples, B. Gu, S. Karan, A. Bismarck, A.G. Livingston,

Organic fouling behaviour of structurally and chemically different forward osmosis membranes: A study of cellulose triacetate and thin film composite membranes, J. Memb. Sci. 520 (2016) 247–261. doi:10.1016/j.memsci.2016.07.065.

[31] B. Mi, M. Elimelech, Organic fouling of forward osmosis membranes: Fouling reversibility and cleaning without chemical reagents, J. Memb. Sci. 348 (2010) 337–345. doi:10.1016/j.memsci.2009.11.021.

[32] P. Bacchin, P. Aimar, R.W. Field, Critical and sustainable fluxes: Theory, experiments and applications, J. Memb. Sci. 281 (2006) 42–69. doi:10.1016/j.memsci.2006.04.014.

[33] S.P. Beier, G. Jonsson, Critical flux determination by flux-stepping, AIChE J. 56 (2010) 1739–1747. doi:10.1002/aic.

[34] Y. Wang, F. Wicaksana, C.Y. Tang, A.G. Fane, Direct Microscopic Observation of Forward Osmosis Membrane Fouling, Environ. Sci. Technol. 44 (2010) 7102–7109. doi:10.1021/es101966m.

[35] S. Zou, Y. Gu, D. Xiao, C.Y. Tang, The role of physical and chemical parameters on forward osmosis membrane fouling during algae separation, J. Memb. Sci. 366 (2011) 356–362. doi:10.1016/j.memsci.2010.10.030.

[36] G. Blandin, H. Vervoort, P. Le-Clech, A.R.D. Verliefde, Fouling and cleaning of high permeability forward osmosis membranes, J. Water Process Eng. 9 (2016) 161–169. doi:10.1016/j.jwpe.2015.12.007.

[37] T.P.N. Nguyen, B.M. Jun, J.H. Lee, Y.N. Kwon, Comparison of integrally asymmetric and thin film composite structures for a desirable fashion of forward osmosis membranes, J. Memb. Sci. 495 (2015) 457–470. doi:10.1016/j.memsci.2015.05.039.

[38] S.J. Kim, S. Kook, B.E. O'Rourke, J. Lee, M. Hwang, Y. Kobayashi, R. Suzuki, I.S. Kim, Characterization of pore size distribution (PSD) in cellulose triacetate (CTA) and

polyamide (PA) thin active layers by positron annihilation lifetime spectroscopy (PALS) and fractional rejection (FR) method, J. Memb. Sci. 527 (2017) 143–151. doi:10.1016/j.memsci.2016.12.064.

[39] J. Lee, S. Kook, C. Lee, I.S. Kim, Effect of intermittent pressure-assisted forward osmosis (I-PAFO) on organic fouling, Desalination. 419 (2017) 60–69. doi:10.1016/j.desal.2017.06.003.

[40] N.Y. Yip, A. Tiraferri, W.A. Phillip, J.D. Schiffman, M. Elimelech, High Performance Thin-Film Composite Forward Osmosis Membrane, Environ. Sci. Technol. (2010). doi:10.1021/es1002555.

[41] M.M. Motsa, B.B. Mamba, A.R.D. Verliefde, Combined colloidal and organic fouling of FO membranes: The influence of foulant-foulant interactions and ionic strength, J. Memb. Sci. 493 (2015) 539–548. doi:10.1016/j.memsci.2015.06.035.

[42] C. Boo, S. Lee, M. Elimelech, Z. Meng, S. Hong, Colloidal fouling in forward osmosis: Role of reverse salt diffusion, J. Memb. Sci. 390–391 (2012) 277–284. doi:10.1016/j.memsci.2011.12.001.

[43] S. Zou, Y.N. Wang, F. Wicaksana, T. Aung, P.C.Y. Wong, A.G. Fane, C.Y. Tang, Direct microscopic observation of forward osmosis membrane fouling by microalgae: Critical flux and the role of operational conditions, J. Memb. Sci. 436 (2013) 174–185. doi:10.1016/j.memsci.2013.02.030.

[44] C.Y. Tang, Q. She, W.C.L. Lay, R. Wang, A.G. Fane, Coupled effects of internal concentration polarization and fouling on flux behavior of forward osmosis membranes during humic acid filtration, J. Memb. Sci. 354 (2010) 123–133. doi:10.1016/j.memsci.2010.02.059.

[45] M.M. Motsa, B.B. Mamba, A. D'Haese, E.M.V. Hoek, A.R.D. Verliefde, Organic fouling

826 in forward osmosis membranes: The role of feed solution chemistry and membrane
827 structural properties, J. Memb. Sci. 460 (2014) 99–109.
828 doi:10.1016/j.memsci.2014.02.035.
829 [46] Q. She, X. Jin, Q. Li, C.Y. Tang, Relating reverse and forward solute diffusion to
830 membrane fouling in osmotically driven membrane processes, Water Res. 46 (2012)
831 2478–2486. doi:10.1016/j.watres.2012.02.024.
832 [47] W.S. Ang, M. Elimelech, Protein (BSA) fouling of reverse osmosis membranes:
833 Implications for wastewater reclamation, J. Memb. Sci. 296 (2007) 83–92.
834 doi:10.1016/j.memsci.2007.03.018.
835 [48] B. Mi, M. Elimelech, Chemical and physical aspects of organic fouling of forward osmosis
836 membranes, J. Memb. Sci. 320 (2008) 292–302. doi:10.1016/j.memsci.2008.04.036.
837 [49] Y. Gu, Y.N. Wang, J. Wei, C.Y. Tang, Organic fouling of thin-film composite polyamide
838 and cellulose triacetate forward osmosis membranes by oppositely charged
839 macromolecules, Water Res. 47 (2013) 1867–1874. doi:10.1016/j.watres.2013.01.008.
840 [50] C. Kim, S. Lee, S. Hong, Application of osmotic backwashing in forward osmosis:
841 Mechanisms and factors involved, Desalin. Water Treat. 43 (2012) 314–322.
842 doi:10.1080/19443994.2012.672215.
843 [51] M. Xie, S.R. Gray, Gypsum scaling in forward osmosis: Role of membrane surface
844 chemistry, J. Memb. Sci. 513 (2016) 250–259. doi:10.1016/j.memsci.2016.04.022.
845 [52] Y. Liu, B. Mi, Effects of organic macromolecular conditioning on gypsum scaling of
846 forward osmosis membranes, J. Memb. Sci. 450 (2014) 153–161.
847 doi:10.1016/j.memsci.2013.09.001.
848 [53] M. Xie, L.D. Nghiem, W.E. Price, M. Elimelech, Impact of organic and colloidal fouling
849 on trace organic contaminant rejection by forward osmosis: Role of initial permeate flux,

Desalination. 336 (2014) 146–152. doi:10.1016/j.desal.2013.12.037.

[54] E. Arkhangelsky, F. Wicaksana, A.A. Al-Rabiah, S.M. Al-Zahrani, R. Wang, Understanding the interaction between biomacromolecules and their influence on forward osmosis process, Desalination. 385 (2016) 12–23. doi:10.1016/j.desal.2016.02.006.

[55] B. Mi, M. Elimelech, Silica scaling and scaling reversibility in forward osmosis, DES. 312 (2013) 75–81. doi:10.1016/j.desal.2012.08.034.

[56] A.S. Kim, E.M. V Hoek, Cake Structure in Dead-End Membrane Filtration: Monte Carlo Simulations, Environ. Eng. Sci. 19 (2002) 373–386. doi:10.1089/109287502320963373.

[57] J.C. Chen, M. Elimelech, A.S. Kim, Monte Carlo simulation of colloidal membrane filtration: Model development with application to characterization of colloid phase transition, J. Memb. Sci. 255 (2005) 291–305. doi:10.1016/j.memsci.2005.02.004.

[58] S. Lee, C. Boo, M. Elimelech, S. Hong, Comparison of fouling behavior in forward osmosis (FO) and reverse osmosis (RO), J. Memb. Sci. 365 (2010) 34–39. doi:10.1016/j.memsci.2010.08.036.

[59] M. Zhang, Q. She, X. Yan, C.Y. Tang, Effect of reverse solute diffusion on scaling in forward osmosis: A new control strategy by tailoring draw solution chemistry, Desalination. 401 (2017) 230–237. doi:10.1016/j.desal.2016.08.014.

[60] E. Arkhangelsky, F. Wicaksana, C. Tang, A.A. Al-Rabiah, S.M. Al-Zahrani, R. Wang, Combined organic-inorganic fouling of forward osmosis hollow fiber membranes, Water Res. 46 (2012) 6329–6338. doi:10.1016/j.watres.2012.09.003.